Optical Spectroscopy of Nicotinoprotein Alcohol Dehydrogenase from *Amycolatopsis methanolica*: A Comparison with Horse Liver Alcohol Dehydrogenase and UDP-Galactose Epimerase[†]

Sander R. Piersma,*[,‡] Antonie J. W. G. Visser,[§] Simon de Vries,[‡] and Johannis A. Duine[‡]

Department of Microbiology and Enzymology, Delft University of Technology, Julianalaan 67, 2628 BC Delft, The Netherlands, and Microspectroscopy Center, Department of Biomolecular Sciences, Agricultural University Wageningen, Dreijenlaan 3, 6703 HA Wageningen, The Netherlands

Received August 25, 1997; Revised Manuscript Received November 10, 1997

ABSTRACT: The NADH absorbance spectrum of nicotinoprotein (NADH-containing) alcohol dehydrogenase from *Amycolatopsis methanolica* has a maximum at 326 nm. Reduced enzyme-bound pyridine dinucleotide could be reversibly oxidized by acetaldehyde. The fluorescence excitation spectrum for NADH bound to the enzyme has a maximum at 325 nm. Upon excitation at 290 nm, energy transfer from tryptophan to enzyme-bound NADH was negligible. The fluorescence emission spectrum (excitation at 325 nm) for NADH bound to the enzyme has a maximum at 422 nm. The fluorescence intensity is enhanced by a factor of 3 upon binding of isobutyramide ($K_d = 59\ \mu M$). Isobutyramide acts as competitive inhibitor ($K_i = 46\ \mu M$) with respect to the electron acceptor NDMA (*N*,*N*-dimethyl-*p*-nitrosoaniline), which binds to the enzyme containing the reduced cofactor. The nonreactive substrate analogue trifluoroethanol acts as a competitive inhibitor with respect to the substrate ethanol ($K_i = 1.6\ \mu M$), which binds to the enzyme containing the oxidized cofactor. Far-UV circular dichroism spectra of the enzyme containing NADH and the enzyme containing NAD^+ were identical, indicating that no major conformational changes occur upon oxidation or reduction of the cofactor. Near-UV circular dichroism spectra of NADH bound to the enzyme have a minimum at 323 nm ($\Delta\epsilon = -8.6\ M^{-1}\ cm^{-1}$). The fluorescence anisotropy decay of enzyme-bound NADH showed no rotational freedom of the NADH cofactor. This implies a rigid environment as well as lack of motion of the fluorophore. The average fluorescence lifetime of NADH bound to the enzyme is 0.29 ns at 20 °C and could be resolved into at least three components (in the range 0.13−0.96 ns). Upon binding of isobutyramide to the enzyme-containing NADH, the average excited-state lifetime increased to 1.02 ns and could be resolved into two components (0.37 and 1.11 ns). The optical spectra of NADH bound to nicotinoprotein alcohol dehydrogenase have blue-shifted maxima compared to other NADH−dehydrogenase complexes, but comparable to that observed for NADH bound to horse liver alcohol dehydrogenase. The fluorescence lifetime of NADH bound to the nicotinoprotein is very short compared to enzyme-bound NADH complexes, also compared to NADH bound to horse liver alcohol dehydrogenase. The cofactor−protein interaction in the nicotinoprotein alcohol dehydrogenase active site is more rigid and apolar than that in horse liver alcohol dehydrogenase. The optical properties of NADH bound to nicotinoprotein alcohol dehydrogenase differ considerably from NADH (tightly) bound to UDP-galactose epimerase from *Escherichia coli*. This indicates that although both enzymes have NAD(H) as nonexchangeable cofactor, the NADH binding sites are quite different.

Nicotinoproteins are, in analogy to flavoproteins and metalloproteins, proteins which contain nicotinamide adenine dinucleotide [NAD(P)(H)] as a cofactor (*1*). The cofactor remains bound to the protein during catalysis unlike a coenzyme, a role usually fulfilled by NAD(P)H. Nicotinoprotein alcohol dehydrogenase (alcohol:*N*,*N*-dimethyl-4-nitrosoaniline oxidoreductase, np-ADH[1] previously called NDMA-ADH) from *Amycolatopsis methanolica* is an enzyme which contains nondissociable, redox-active NADH as cofactor. The enzyme catalyzes the reversible, NAD^+-independent oxidation of primary alcohols with the concomitant reduction of the artificial electron acceptor *N*,*N*-dimethyl-*p*-nitrosoaniline (NDMA) (*2*). The pyridine dinucleotide of np-ADH does not dissociate from the enzyme during catalysis, purification or dialysis. From N-terminal

[†] The investigations were supported by The Netherlands Foundation for Chemical Research (SON) with financial aid from The Netherlands Organization for Scientific Research (NWO).

* To whom correspondence should be addressed. Fax: 31 15 2782355. E-mail: s.r.piersma@stm.tudelft.nl.

[‡] Delft University of Technology.

[§] Agricultural University Wageningen.

[1] Abbreviations: IBA, isobutyramide; LADH, horse liver (*Equus cabalus*) alcohol dehydrogenase (EE isoenzyme); MEM, maximum entropy method; NDMA, *N*,*N*-dimethyl-*p*-nitrosoaniline; np-ADH, nicotinoprotein [NAD(H) containing] alcohol dehydrogenase from *Amycolatopsis methanolica*; TFE, trifluoroethanol; YADH, yeast (*Saccharomyces cerevisiae*) alcohol dehydrogenase (I); alcohol dehydrogenase (EC 1.1.1.1); NDMA-dependent alcohol dehydrogenase (EC 1.1.99.-).

S0006-2960(97)02115-6 CCC: $15.00
Published on Web 02/10/1998

sequence determinations, a sequence identity of 50% was found with the well characterized class I horse liver alcohol dehydrogenase (LADH).

The nicotinoprotein for which most mechanistic, structural, and spectroscopical data is available is UDP-galactose epimerase, an enzyme which contains nondissociable NAD^+ and which catalyzes the nonstereospecific epimerization of UDP-galactose to UDP-glucose (*3*−*6*). A comparison of the nicotinoproteins np-ADH and UDP-galactose epimerase could show whether the tight binding of the pyridine dinucleotide in the active sites of both enzymes is reflected in the optical properties of the reduced cofactor bound to the enzymes.

Since the optical properties, such as UV−vis absorbance, fluorescence, and elliptical rotation, of the LADH−NADH binary complex and several ternary complexes have been reported and partially assigned to structural features (*7*), a comparative study of native np-ADH (and complexes of this enzyme with inhibitors) with the binary and ternary LADH complexes could yield information on both the active site environment and the NADH binding site of np-ADH. Enzyme-bound NADH is a sensitive natural fluorescent probe of the active site environment (*8, 9*). Especially, time-resolved fluorescence has been applied to dehydrogenase-bound dihydronicotinamides during the last two decades (*10*−*13*). It has also been applied to the nicotinoprotein UDP-galactose 4-epimerase to yield information on the NADH environment of the enzyme (*4*). The time-resolved fluorescence properties of the LADH−NADH binary complex and ternary complexes with isobutyramide have been reported (*13*−*15*). The fluorescence decay kinetics could be resolved into two or even more fluorescence lifetimes, but there is no consensus about the origin of this heterogeneity (*13, 14, 16, 17*). The multiexponential decay of NADH bound to LADH has been interpreted recently as a reversible excited-state reaction (*13*).

We want to know the nature of dinucleotide binding in nicotinoproteins in relation to NAD^+-dependent enzymes. In this paper, the analysis of the fluorescence decay and fluorescence anisotropy decay kinetics of NADH bound to np-ADH will be described and a comparison with the LADH−NADH binary and ternary complexes and with UDP-galactose epimerase will be made. In addition to the optical properties of np-ADH also, the inhibition constants of ADH inhibitors acting on np-ADH will be evaluated in relation to enzymological data obtained for np-ADH and literature data of class I NAD^+-dependent alcohol dehydrogenases.

MATERIALS AND METHODS

Materials. The fluorescence reference compound xanthione was dissolved in hexane prior to measurements. NADH was obtained from Merck (grade I); an absorbance coefficient of 6.22 mM^{-1} cm^{-1} at 340 nm was used to determine the concentration of the coenzyme in aqueous solution. Chemicals were of the highest quality available and they were used without further purification. Horse liver ADH was purchased from Sigma but was further purified prior to use. The crystalline preparation was dissolved in a 100 mM potassium phosphate buffer, pH 7.0, and dialyzed against 1000 vol of the same buffer. This was followed by centrifugation to remove any insoluble material. The LADH concentration was determined using an absorbance coefficient at 280 nm of 38.2 mM^{-1} cm^{-1}. LADH−NADH binary complex was prepared using a 4:1 stoichiometry for LADH versus NADH to ensure >98% complex formation. Steady-state and time-resolved fluorescence experiments were performed in 100 mM potassium phosphate buffer, pH 7.0. If not specified, the temperature was 20 ± 1 °C. The OD_{340} or OD_{325} was <0.1 for all preparations used in fluorescence experiments to eliminate inner filter effects. Both np-ADH−IBA and LADH−NADH−IBA complexes were made in 100 mM isobutyramide (final concentration) supplemented to the phosphate buffer. The water used in both experiments and enzyme purification was of >18 MΩ/cm quality (milliQ, Millipore) and was filtered through a 0.22 μm filter prior to use.

Enzyme Purification. np-ADH was isolated from cell-free extract of methanol (1% v/v) grown *Amycolatopsis methanolica* essentially as described previously (*2*). There were small modifications in the isolation procedure of the enzyme. The first step was a DEAE Bio-Gel agarose anion exchange column (Bio-Rad). The enzyme was eluted with a sodium chloride gradient (0 to 1.0 M in 50 mM MOPS, pH 7.8; elution of np-ADH occurred at 300 mM NaCl; temperature 4 °C) after which the phenyl sepharose and mono-Q steps followed as described by van Ophem et al. (1993). The hydroxyapatite step was, however, omitted. The final gel filtration step was performed on a Superdex-200 column (Pharmacia). The final buffer in the gel filtration step was 100 mM potassium phosphate, pH 7.0, which is identical with the buffer used in fluorescence experiments. Purity of the enzyme preparation was confirmed by a single band on SDS−PAGE (*18*) and was also checked with the data analysis software of the HPLC system (HP Chemstation 3D) during the final purification step.

Activity Measurements. The activity of np-ADH was determined by monitoring the decrease in absorbance of NDMA at 440 nm in a 1 mL volume containing 100 mM potassium phosphate buffer, pH 7.0 and 1 mM ethanol, 20 °C. The concentration of NDMA was determined from the absorbance at 440 nm using an absorbance coefficient of 35.4×10^3 M^{-1} cm^{-1} (*19*). Absorbance changes and optical absorbance spectra were recorded with a Hewlett-Packard 8452 A diode array spectrophotometer. Competitive inhibition of isobutyramide with respect to NDMA was investigated by monitoring the activity with varying concentrations of NDMA at several fixed concentrations of IBA, keeping the alcohol concentration at 1 mM. Inhibition by trifluoroethanol was investigated in a similar fashion with respect to ethanol, keeping the NDMA concentration at 28 μM. Kinetic data sets were fitted to the appropriate equations using the enzyme kinetics fitting program LEONORA (*20*).

Spectroscopy. Optical absorbance spectra were recorded with an HP 8452 A diode array spectrophotometer (2 nm resolution) using a 1.0 cm quartz cuvette. Spectra obtained from gel filtration experiments were recorded during elution with an HP 1040 HPLC diode array detector (2 nm resolution, 6 mm path length). The specific absorbance coefficient was calculated from the ratio A_{280}/A_{205} obtained during a gel filtration experiment in which the pure protein was injected in the column and the absorbance was monitored from 190 to 400 nm. The specific absorbance coefficient was calculated according to established procedures (*21*).

Circular dichroism spectra were recorded for the far-UV between 190 and 240 nm and for the near-UV between 270 and 370 nm for the peptide and chromophore region, respectively, with a Jobin-Yvon Mark V dichrograph. The cuvettes used had a path length of 0.01 and 1.0 cm, respectively. The scan speed was 0.055 nm s^{-1}; the spectra consisted of 500 or 1000 data points (for the far-UV and near-UV respectively). Secondary structure calculations from the far-UV CD data were performed with the CONTIN computer program (*22*). In the calculations, the amount of peptide bonds was estimated from the monomer molecular mass, 39 kDa, to be 360. The fitting procedure however, is not very sensitive to small changes in the number of peptides or the absolute concentrations used in the calculations. The Gaussian band calculated from the near UV spectrum was obtained using the IGOR-pro data processing program (Wave metrics). In all CD experiments, the buffer blank was recorded separately and subtracted from the sample spectrum.

Steady-state emission and excitation fluorescence spectra in the NADH and tryptophan region were recorded with an SLM Aminco SPF 500 spectrofluorimeter using slit widths of 2 nm both in excitation and emission wavelengths. In all fluorescence experiments the buffer blank containing the water Raman signal was recorded separately and subtracted from the sample spectrum.

The dissociation coefficient for isobutyramide was determined with a fluorescence enhancement titration experiment. Small volumes of a concentrated stock solution isobutyramide were added to the enzyme, and the fluorescence emission was recorded upon excitation at 325 nm.

Time-resolved fluorescence measurements were performed with the time correlated single-photon counting method in an instrumental setup described earlier (*23*, *24*). A mode locked cw YLF laser (Coherent model Antares 76-YLF) equipped with an LBO frequency doubler was used for the synchronously pumping of a cavity-dumped Rhodamine 6G (tryptophan) or DCM (NADH) dye laser (Coherent model 701-2 CD). The output was frequency doubled with a BBO crystal to yield the vertically polarized excitation beam. The repetition rate of the excitation pulses was 951 kHz. The excitation wavelength was 295 nm for tryptophan and 340 nm for NADH fluorescence. The NADH emission wavelengths were selected using a WG370 cutoff filter (Schott) and an interference filter at 392.1, 422.0, or 480.5 nm, respectively (Schott). Perpendicular and parallel components (with respect to the direction of the excitation beam polarization) of the fluorescence were selected with a sheet type polarizer (Polaroid type HNP′B) which could be rotated under computer control. The single photon counting signal was obtained with a microchannel-plate photomultiplier (Hamamatsu, model 1645U) and was after amplification transferred to a time to amplitude converter (TAC) (Tennelec TC 846). The analogue TAC output signal was converted into a digital signal (Nuclear Data model ND 582) and was stored in a multichannel analyzer. The experimental decay was stored in 1000 channels with 20 ps/channel. The instrumental response function was determined by measuring the rapid fluorescence decay of the reference compound xanthione dissolved in *n*-hexane. NADH fluorescence was sampled 10 cycles of 10 s in both polarization directions. The detection frequency of the parallel polarized component was set to 30 kHz (3% of excitation frequency) to prevent pulse pileup. The reference compounds were sampled 3 cycles of 10 s, and the background (buffer without protein) was sampled 2 cycles of 10 s in both polarization directions. The temperature was maintained at the indicated temperature using an Oxford instruments ITC 4 temperature controller.

Data Analysis. The fluorescence decay $f(t)$ can be analyzed in terms of a series of exponentials:

$$f(t) = \sum_j \alpha_j e^{-t/\tau_j} \tag{1}$$

in which τ_j is the fluorescence lifetime and α_j is the preexponential amplitude factor. Analysis of the fluorescence anisotropy decay was performed with the commercially available maximum entropy method (MEM, Cambridge, U.K.). Details of the analysis method are described elsewhere (*25*). For the analysis of the fluorescence decay into a distribution of fluorescence lifetimes τ with amplitudes α, 100 equally spaced values on a $\log(\tau)$ scale between 0.01 and 10 ns were used. The starting distribution model was chosen to be flat in $\log(\tau)$ space: all fluorescence lifetimes have equal probability, since no a priori knowledge about the system is present. The quality of fluorescence decay and anisotropy decay analyses were evaluated by inspection of the weighted residuals and the autocorrelation function of the residuals, which both should be randomly distributed around the zero line, and the value of the reduced χ^2, which should be minimized close to unity. The sum of the preexponential amplitude factors has been normalized to one for presentation of the data in the tables.

The anisotropy $r(t)$ of fluorescence is defined as

$$r(t) = \frac{i_{||}(t) - i_{\perp}(t)}{i_{||}(t) - 2i_{\perp}(t)} \tag{2}$$

in which $i_{||}$ and $i_{\perp}$ are the parallel and perpendicular components of the fluorescence decay. The fluorescence anisotropy decay can also be analyzed with the maximum entropy method analogous to that of the fluorescence decay. Details are given elsewhere (*23*). In a typical protein system containing fluorescent groups, the anisotropy decay can be composed of a fast internal motion of the bound fluorophore (characterized by ϕ_{int}) and a much slower protein rotation (characterized by ϕ_{prot}). The Debye−Stokes−Einstein relationship between the protein rotational correlation time φ_{prot} and a spherical symmetric rotor is given by

$$\varphi_{prot} = \frac{\eta V}{kT} = \frac{\eta M(\bar{v} + h)}{RT} \tag{3}$$

where η is the viscosity of the solvent (cP), V is the hydrodynamic volume of the rotor, k is the Boltzmann constant, R is the gas constant, and T is the absolute temperature. It is possible to estimate the protein rotational correlation time φ_{prot} if the molecular mass (M) of the protein is known. If the protein is considered to be a rigid hydrated sphere, the volume V from eq 3 can be replaced with $m(\bar{v} +$ h), in which $\bar{v}$ is the partial specific volume (0.735 cm^3 g^{-1}) and h is the degree of hydration (0.2 cm^3 g^{-1}).

RESULTS

Competitive Inhibitors. Isobutyramide (IBA) binds selectively to LADH with bound reduced coenzyme and forms

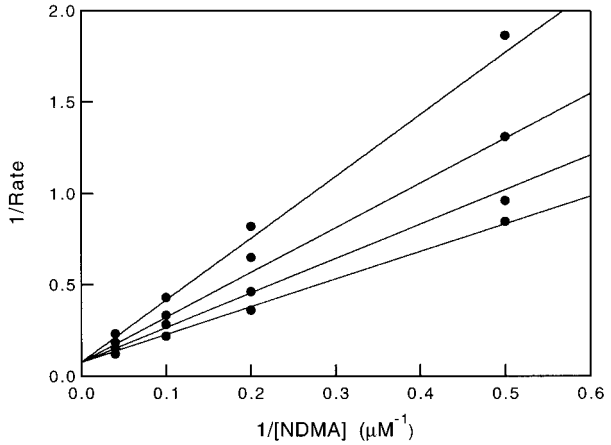

FIGURE 1: Competitive inhibition by isobutyramide. The enzyme activity was determined as described in Materials and Methods. Markers indicate experimental data points, lines indicate simulations using fitted parameters from reversible competitive inhibition calculated for the whole dataset using the fitting program LEONORA. Isobutyramide concentrations: 100, 50, 25, and 10 μM, ethanol was fixed at 1 mM.

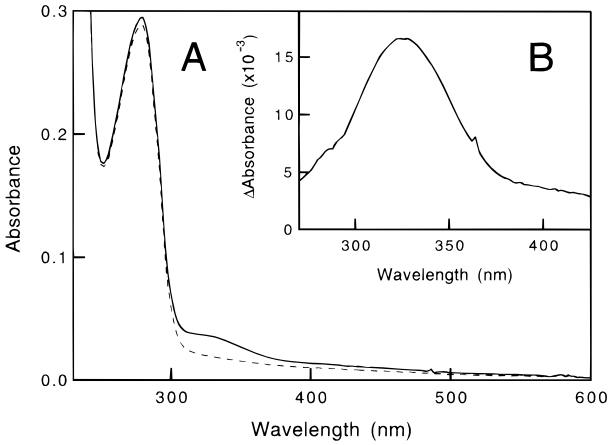

FIGURE 2: UV and visible absorbance spectra of 7.3 μM np-ADH. The solid line in panel A shows the reduced np-ADH, the dotted line shows the oxidized enzyme (after addition of 10 mM acetaldehyde). Panel B shows the reduced minus oxidized difference spectrum having a maximum at 326 nm.

a tightly bound LADH−NADH−IBA ternary complex (*26*). IBA acts as inhibitor of np-ADH, it can also form a ternary complex with this enzyme having the reduced pyridine dinucleotide as cofactor. IBA is a competitive inhibitor of the enzyme with respect to the electron acceptor NDMA as illustrated by intersecting lines in a plot of the reciprocal initial rates versus the reciprocal concentrations of substrate (NDMA) at varying concentrations of inhibitor (IBA) as shown in Figure 1.

Since the mechanism of np-ADH is ping-pong, the Lineweaver−Burke plot should give intersecting lines at $1/[S] = 0$ for competitive inhibition (Figure 1). The value of K_i was calculated using eq 4 giving a K_i of 46 μM for IBA at a fixed concentration of ethanol (1 mM). Trifluoro-

$$\frac{v}{[e]} = \frac{k_{cat}[S]}{K_m(1 + [I]/K_i) + [S]} \quad (4)$$

ethanol (TFE) is a nonreactive substrate analogue which forms a tight complex with LADH and NAD^+ (*27*). It acts as competitive inhibitor of LADH with respect to ethanol. It can also act as an inhibitor for np-ADH. TFE is a competitive inhibitor with respect to ethanol in the oxidation of ethanol by np-ADH with NDMA. The same pattern as in the case of IBA is seen (Figure 1), however. The NDMA concentration is kept constant (28 μM) in this case, and the ethanol concentration is varied. The K_i of TFE is 1.65 μM, indicating a high affinity of np-ADH for this substrate analogue.

Absorbance Spectroscopy. The optical absorbance maximum of the enzyme-bound chromophore NADH is not well resolved from the protein absorbance band in the normal absorbance spectrum of the reduced enzyme (*2*). The ethanol-free enzyme containing NADH could be oxidized reversibly with an excess of acetaldehyde. The reduced minus oxidized difference spectrum (Figure 2) clearly shows the NADH absorbance maximum at 326 nm. The Gaussian bandwidth of the absorbance band in the difference spectrum (33 nm) is comparable to the 340 nm band of NADH in aqueous solution (34 nm). The enzyme obtained after the final isolation step contains NADH. The absorbance maximum of enzyme-bound NADH at 326 nm is blue shifted compared to the absorbance maximum of NADH in water being 340 nm.

The specific absorbance coefficient was obtained from the optical spectra of the pure protein (pure according to the peak-purity criteria of the HP Chemstation software and to SDS−PAGE gel electrophoresis) taken during elution of the protein from the gelfiltration column. The absorbances at 205 and 280 nm during peak elution were extracted from the data set, and the mean value of A_{280}/A_{205} through the peak was used in the calculation of the specific absorbance coefficient (*21*). The specific absorbance coefficient $A^{0.1\%}_{280nm}$ calculated for np-ADH is 0.988 mg^{-1}, which corresponds to a molar subunit absorbance coefficient at 280 nm of 39.5×10^3 M^{-1} cm^{-1} (using a subunit molecular mass of 39 kDa, which was obtained from SDS−PAGE). The absorbance coefficient of 39.5×10^3 M^{-1} cm^{-1} at 280 nm was used to determine the np-ADH concentrations in the other experiments. In pure, fresh preparations of the enzyme, the NADH absorbance band is moderately resolved from the protein absorbance band and displays a maximum at 326 nm, in older preparations and after several cycles of freezing and thawing resolution from the protein absorbance band decreases (SDS−PAGE analysis gave identical patterns). The ratio A_{326}/A_{280} in fresh preparations eluting from the gelfiltration column in the final purification step is 0.14.

Circular Dichroism. The near-UV CD spectra between 270 and 370 nm of np-ADH and of NADH of comparable concentration are given in Figure 3. The CD spectrum of np-ADH consists of a well-defined negative near Gaussian band at 323 nm and a less-defined band at 292 nm. The small negative band at 292 nm can be attributed to aromatic amino acid residues, most probably tryptophan (the tryptophan fluorescence excitation maximum of np-ADH is also located at 292 nm). The 323 nm band corresponds to the 326 nm band attributed to the NADH absorbance in the absorbance spectrum of the np-ADH. The major negative Cotton band has a molar ellipticity $\Delta\epsilon$ at 323 nm of −8.6 M^{-1} cm^{-1} (using the absorbance coefficient at 280 nm) with a Gaussian half bandwidth of 35.1 nm [the Gaussian band shape was adopted from Wong et al. (*5*)]. The value for $\Delta\epsilon$

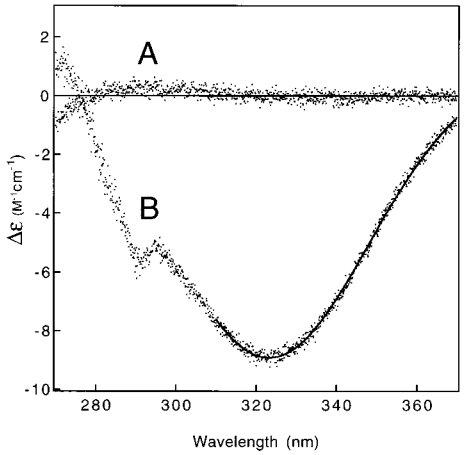

FIGURE 3: Circular dichroism spectra of 27.9 μM NADH (A) and 29.6 μM np-ADH (B) (dots). The solid line is a Gaussian fit to the np-ADH spectrum (from 310 to 370 nm)

Table 1: Secondary Structure Content of Oxidized[a] and Reduced np-ADH[b]

secondary structure	E:NADH	E:NADH (w)	E:NAD$^+$	E:NAD$^+$ (w)
α-helix	31 (1.2)	29 (0.8)	29 (0.8)	30 (0.5)
β-sheet	29 (3.6)	31 (2)	32 (2.6)	32 (1.7)
β-turn	23 (2)	21 (1)	19 (1.2)	18 (0.8)
random coil	17 (2)	19 (1)	20 (1.1)	20 (0.7)

[a] The oxidized enzyme was obtained by addition of 10 mM acetaldehyde (final concentration). [b] The enzyme concentration in the experiment is 29.6 μM. The spectra were analyzed for secondary structure using the 16 CD spectra of proteins with a known 3-D structure as a basis set. The fits were verified by inspection of the residuals, random fluctuations around zero indicated a good fit. In the columns indicated with (w), the signal was weighed during the fitting procedure in the 190−200 region (because of low signal-to-noise ratio). Values in parentheses are the standard errors.

is in the same order of magnitude as NADH bound to LADH (−13 M^{-1} cm^{-1}, λ_{max} 325 nm) and much larger than $\Delta\epsilon$ for NADH in solution (0.03 M^{-1} cm^{-1}, λ_{max} 340 nm) (*7*). The rotational strength of the enzyme bound chromophore indicates the presence of asymmetric interactions involving the 323 nm transition.

The far-UV CD spectra (not shown) of both the oxidized and the reduced enzyme were also recorded to check for possible major protein conformational changes upon oxidation and reduction of the pyridine dinucleotide chromophore. The maximum ellipticity is observed at ca. 195 nm. In the 200−240 nm region, two minima are observed, the largest one at ca. 210 nm and a smaller minimum at ca. 222 nm, both minima are indicative of the presence of α-helix-type secondary structure. In the far-UV region, the secondary structure elements of the protein can be probed. The secondary structure is analyzed in percent of the basic elements α-helix, β-sheet, β-turn, and random coil. The results of the analysis are given in Table 1. No large conformational change is observed upon oxidation or reduction of the chromophore. Local conformational changes may, of course, occur while leaving the secondary structure blocks essentially unaltered.

Steady-State Fluorescence. The tryptophan fluorescence of the oxidized and reduced np-ADH were recorded (not shown) and showed emission maxima at 339 nm and excitation maxima at 292 nm, the steady-state fluorescence of the tryptophan residues is not much affected by the redox state of the pyridine dinucleotide or by binding of IBA to the reduced enzyme, the intensity of the fluorescence being approximately 5% lower upon oxidation of the dihydronicotinamide. Upon excitation at 295 nm of reduced np-ADH, only the 339 nm tryptophan fluorescence band is present without significant additional features at higher wavelengths. This is in contrast to the LADH−NADH binary complex where a clear emission at 400−450 nm can be observed (under identical conditions, data not shown) in addition to the 340 nm tryptophan emission and which is to be attributed to resonance energy transfer from tryptophan to enzyme-bound NADH (*28*). In addition to the steady-state tryptophan fluorescence, time-resolved fluorescence shows that the fluorescence lifetime of Trp in np-ADH is also hardly affected by the oxidation state of the pyridine dinucleotide. This indicates that the tryptophans present in np-ADH are not in the appropriate geometry to facilitate efficient energy transfer (the relative angles of the transition dipole moments of NADH and tryptophan are probably unfavorable and/or the distance is too large).

Steady-state fluorescence excitation and emission spectra of np-ADH, containing the reduced chromophore and its complex with NADH and isobutyramide, respectively, were recorded (Figure 4). The steady-state fluorescence of the enzyme-bound NADH has an emission maximum at 422 nm and an excitation maximum at 326 nm, in addition to the excitation maximum at 280−290 nm probably arising from the high wavelength tail of the tryptophan fluorescence emission. The fluorescence emission of np-ADH-bound NADH is blue-shifted compared to the emission of NADH in solution and also compared to the LADH−NADH binary complex emission being 430 nm. The fluorescence intensity of the enzyme−IBA complex is enhanced, but the emission and excitation maxima remain unchanged. Differences in fluorescence intensity indicated different fluorescence yields. Normalized emission spectra, however, were identical. A change in the shape of the tryptophan fluorescence excitation band can be observed upon emission at 422 nm; the band sharpens and displays a small red shift to a maximum located at 292 nm. The fluorescence yield of NADH bound to np-ADH is somewhat lower compared to the LADH−NADH binary complex at the same $OD_{325\ nm}$ (the same is observed for both ternary complexes with IBA). Figure 4B shows the titration curve of reduced np-ADH with IBA. The fluorescence of enzyme-bound NADH is enhanced by a factor 3 upon binding of IBA. The fluorescence enhancement is calculated with eq 5

$$\Delta F = \frac{\Delta F_{max}[L]}{K_d + [L]} \quad (5)$$

in which ΔF is the observed fluorescence enhancement, ΔF_{max} is the maximal fluorescence enhancement at infinite concentration of ligand and [L] is the free ligand concentration, IBA in this case. The K_d of the enzyme for IBA, calculated from the titration experiment, is 59 μM with a ΔF_{max} of 2.2. Since the enzyme concentration is 10 times smaller than K_d, no correction for L bound to E was made.

Time-Resolved Fluorescence. Fluorescence decay experiments were performed under experimental conditions similar to those employed previously for LADH (*14*) in order to

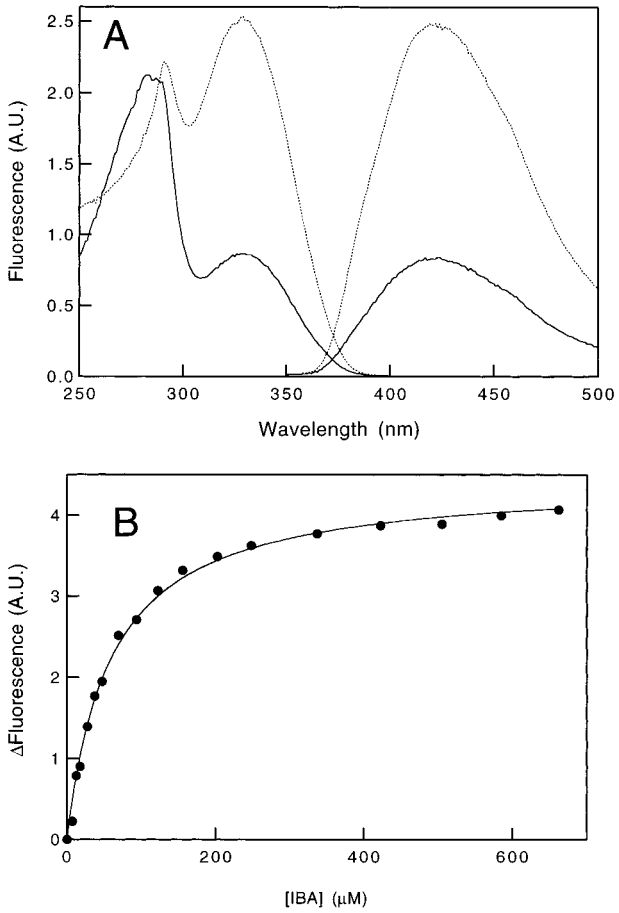

FIGURE 4: (A) Fluorescence excitation (left) and emission (right) spectra of 15 μM np-ADH, emission was monitored at 422 nm and excitation occurred at 325 nm. The solid line is reduced np-ADH, the dotted line is the np-ADH−IBA complex prepared as described in Materials and Methods. The fluorescence intensity is in arbitrary units and all spectra were recorded under identical conditions. (B) Fluorescence enhancement titration of np-ADH with isobutyramide, data points (●) and fit to eq 5 are shown (solid line).

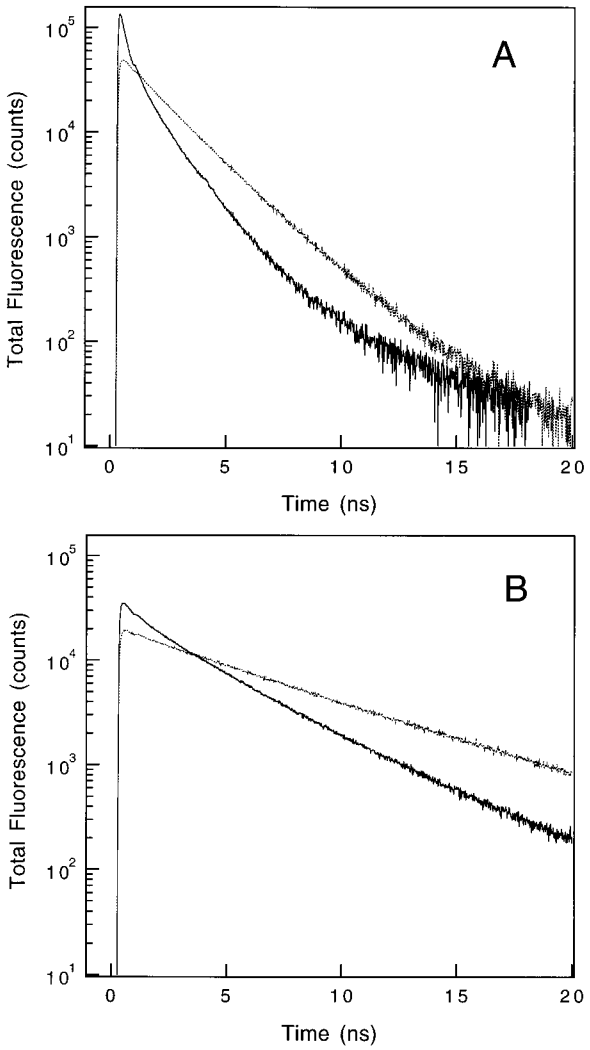

FIGURE 5: Experimental fluorescence decays of np-ADH (A) and LADH (B) at 1 °C. The solid lines are the respective enzyme−NADH complexes, the dotted lines are the enzyme−NADH−IBA complexes. Experimental conditions are identical for all decays.

facilitate a comparison of the results. Both the LADH−NADH binary complex and np-ADH as well as the respective isobutyramide complexes were studied at both 1 and 20 °C.

The NADH emission wavelength was selected in the maximum of np-ADH fluorescence at 422 nm. Excitation occurred at a fixed wavelength (340 nm) at the red edge of the enzyme-bound NADH absorbance band. Inspection of the experimental decay curves shows that the fluorescence decay of np-ADH is faster than the fluorescence decay of the LADH−NADH binary complex both at 1 and at 20 °C. This also holds for the respective isobutyramide complexes (Figure 5). The average fluorescence lifetime is shorter at higher temperatures for both binary and ternary complexes of both enzymes. The fluorescence decay parameters are listed in Table 2. The more heterogeneous character of the np-ADH fluorescence decay is better in agreement with a continuous distribution of fluorescence lifetimes rather than the two distinct lifetimes observed for the LADH−NADH binary complex. The np-ADH−IBA complex however, displays a fluorescence decay curve comparable to those of LADH−NADH and the LADH−NADH−IBA complex in having two distinct fluorescence lifetimes. Isobutyramide stabilizes the excited-state of the enzyme-bound NADH (longer fluorescence lifetime). Our observations with the

Table 2: Fluorescence Decay Parameters of Enzyme-Bound NADH in Binary and Ternary Complexes[a]

ADH complex	T (°C)	lifetimes (ns) α_1	τ_1	α_2	τ_2	α_3	τ_3	$\langle\tau\rangle^b$
LADH−NADH	1	0.24	0.44	0.76	3.16			2.51
LADH−NADH[c]	1	0.58	1.8	0.42	4.2			2.81
LADH−NADH−IBA	1	0.08	0.59	0.16	3.26	0.76	6.39	5.39
LADH−NADH−IBA[c]	1			0.29	2.9	0.71	6.9	5.7
np-ADH	1	0.59	0.16	0.21	0.50	0.20	1.30	0.52
np-ADH−IBA	1	0.07	0.54	0.93	1.85			1.76
LADH−NADH−IBA	20	0.15	0.43	0.85	1.12			1.02
np-ADH	20	0.67	0.13	0.22	0.46	0.11	0.96	0.29
np-ADH−IBA	20	0.13	0.37	0.87	1.11			1.02

[a] Fluorescence decay parameters were determined as described in the Materials and Methods. np-ADH concentration is 15 μM, and for the IBA complex 13.5 μM, LADH concentration is 65 and 58.5 μM for the IBA complex, NADH concentration for LADH−NADH(−IBA) complexes is 15 μM. [b] Average fluorescence lifetime calculated with $\langle\tau\rangle = \sum\alpha_j\tau_j$. [c] Published decay parameters for LADH (*14*). χ^2 for the MEM analyses ranged 1.06−1.38.

LADH complexes are comparable to those made previously (*13*, *14*). However, our analysis resolves the fast decay component in the LADH−NADH−IBA complex (α 29%, τ 2.9 ns at 20 °C) in a low amplitude fast component (α

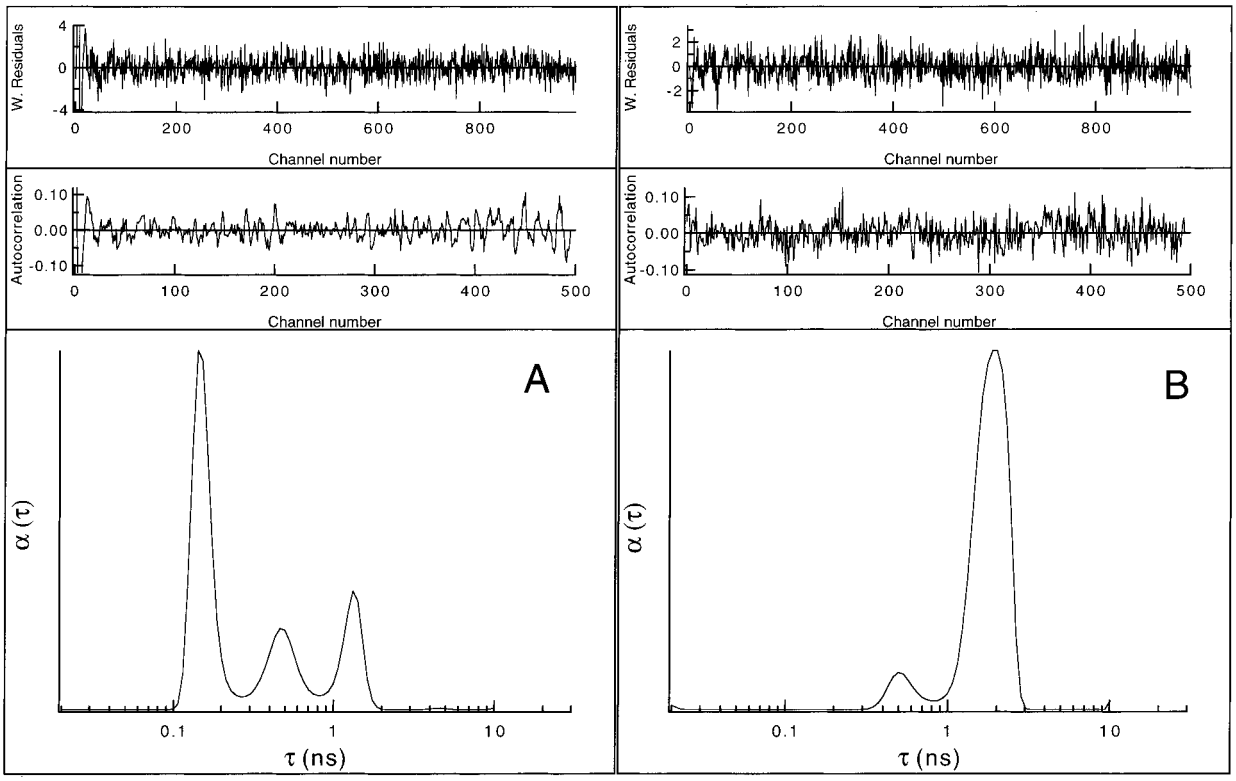

FIGURE 6: Distribution of fluorescence lifetimes of np-ADH (A) and the np-ADH−IBA complex (B) at 1 °C as recovered by maximum entropy analysis (MEM) of the corresponding experimental decays of Figure 5A with weighted residuals between experimental and fitted curves and autocorrelation function of the residuals.

8%, τ 0.59 ns) and a higher amplitude slower component (α 16%, τ 3.26 ns) (Table 5). The differences may, however, be attributed to a different instrumental setup and a different method of data analysis.

Fluorescence Anisotropy Decay. The anisotropy decay of the enzyme-bound NADH in both enzyme complexes (np-ADH and LADH) and both IBA complexes indicated a fully immobilized chromophore for both LADH and np-ADH. No (low amplitude) fast rotations were observed on the (sub-) nanosecond time scale (0.1−5 ns). Since the fluorescence decay is much faster than the protein rotation, it was not possible to determine the protein rotational correlation times accurately. The coenzyme and cofactor are immobilized in the protein matrixes of the respective enzyme active sites. From the expression which correlates molecular mass to rotational correlation times (eq 3), a ϕ of 30 ns is expected for a hydrated sphere with a molecular mass of 80 kDa (LADH), and a ϕ of 60 ns is expected for a similar sphere of 160 kDa. Theoretically, three protein rotation correlation times are expected for an ellipsoid-like protein like LADH depending on the ratio of the axes of the prolate ellipsoid being 1.8 for this enzyme (*29*). A ϕ_{prot} of 33−39 ns was determined from least-squares analysis of the tryptophan fluorescence anisotropy decay of LADH (*29*). However, no resolution was observed in the MEM analyses (0.1−100 ns) of the anisotropy decay of the NADH bound to either LADH or np-ADH in our experiments. As a control, the rotational correlation time of NADH in solution was measured at different temperatures (4, 16, 26, and 35 °C) giving rotational correlation times ranging from 0.1 to 0.3 ns. A linear relationship is obtained for the rotational correlation times ϕ (ns) as a function of the viscosity divided by the absolute temperature and the gas constant (η/RT cP/mol K) indicating that the Debye−Stokes−Einstein law for rotational diffusion can be applied (eq 3). Moreover the slope of the line gives a value of 981 ± 44 Å^3 for the hydrodynamic volume of NADH in solution. These measurements confirm earlier results (*30*) and indicate that NADH in solution is mainly in a folded state.

The anisotropy decay of the tryptophan(s) in np-ADH was also measured in a 50 ns experiment. The tryptophan fluorescence decay is slower than that of enzyme-bound NADH. In this experiment only the local flexibility was observed (ϕ, 0.5−2 ns) for the tryptophan residue(s); no distinct protein rotational correlation time in the 10−100 ns range could be recovered by MEM analysis.

DISCUSSION

Inhibitors of Alcohol Dehydrogenase. The main difference between LADH and np-ADH is the nondissociable nature of enzyme-bound NADH in np-ADH. The difference between NAD^+-dependent alcohol dehydrogenases and nicotinoprotein ADH could be reflected in the dissociation constant and the dissociation rate of enzyme bound NADH. The K_d and k_{off} for NADH differ for class I ADHs. K_d ranges from 48 μM for human $\beta_3\beta_3$ ADH (*31*), 31 μM for yeast ADH I (YADH) (*32*), 3 μM for human $\beta\beta$47Q ADH, 1.2 μM for human $\beta_2\beta_2$ ADH (*33*), and 0.3 μM for LADH (*34*) to 0.01 μM for human $\beta_1\beta_1$ ADH (*33*) (all at pH 7−7.5 and 25−30 °C). For k_{off}, the following values have been reported by the same authors: 23, 590, 10, 5, 6.3, and 0.06 s^{-1} respectively, spanning 4 orders of magnitude. The difference of k_{off} for NADH of the dimeric mammalian class-I ADHs compared to the tetrameric yeast ADH is striking. The rate-limiting step during turnover of ethanol by LADH is release

of NADH, whereas the rate-limiting step is hydride transfer for the yeast enzyme. For UDP-galactose epimerase, it has been reported that the enzyme-bound pyridine dinucleotide has a structural function in addition to its role in catalysis and that it does not exchange with cytosolic NAD(H) (*35*). The pyridine dinucleotide is locked up in the active site of the nicotinoprotein and slow release of NADH from the epimerase does not occur. Since inactivation due to loss of cofactor during purification and dialysis is never observed for np-ADH, we concluded that k_{off} is at least orders of magnitude smaller than that of human $\beta_1\beta_1$ ADH, the slowest NADH releasing ADH, if NADH dissociation actually occurs. It appears that for nicotinoproteins such as np-ADH and UDP-galactose epimerase, no simple two-state equilibrium between apo and holo enzyme exists.

Trifluoroethanol, a nonreactive alcohol substrate, binds to the np-ADH−NAD^+ complex. The competitive inhibition constants for TFE are also reported for LADH (8.4 μM) (*36*) and YADH (2500 μM) (*32*). The yeast enzyme has a much lower affinity for the alcohol analogue than the horse liver enzyme, np-ADH (K_i = 1.65 μM) resembles the LADH active site more, with respect to TFE binding, than that of YADH.

Isobutyramide is a class I ADH inhibitor and it binds to the ADH−NADH complex. The kinetics of IBA acting as competitive inhibitor with respect to the artificial electron acceptor NDMA have been studied for native LADH and LADH with NADH covalently attached via the surface residue Asp-178 (37). K_i values of 270 and 280 μM have been reported for the wild-type and the modified enzyme respectively, values which are 5-fold higher than the K_i of 46 μM obtained for np-ADH. The dissociation constant of IBA with respect to LADH−NADH is 140 μM (*38*), which is 2-fold higher than the K_d of 59 μM obtained for np-ADH. IBA enhances the binding of NADH to LADH with a factor 60 (K_d 0.3 μM vs 5 nM) (*26*). On the basis of inhibition data presented above, the nicotinoprotein np-ADH behaves like a class I ADH, and the active site structure is likely to be more similar to that of LADH than to that of YADH, in agreement with the available sequence information (*2*).

Circular Dichroism: Conformational Changes. In general, a blue-shifted dehydrogenase-bound NADH absorbance is indicative for an A-specific dehydrogenase: only the *re* side hydrogen of C4 of NADH takes part in hydride transfer (*39*). Class I alcohol dehydrogenases are also very stereospecific with respect to the *pro-R* hydrogen of the alcohol substrate. np-ADH is likely to be an A-specific ADH on basis of the blue-shifted NADH absorbance maximum, and it has been shown to be specific for the *pro-R* hydrogen of alcohols (oxidation) and for the *re* side of aldehydes (reduction) (to be published elsewhere). LADH shows a conformational change upon binding of coenzyme (*40*), but upon oxidation and reduction of the coenzyme, when bound to the enzyme, no additional conformational changes occur. This is in contrast to observations reported for UDP-galactose epimerase, where a conformational change is observed upon oxidation and reduction of the cofactor, involving a *syn/anti* rotation of the nicotinamide glycosidic bond, and which is essential in the nonstereospecific catalytic mechanism (*5, 6, 35*). The far-UV circular dichroism spectra of np-ADH, indicative of secondary protein structure, do not show conformational changes upon oxidation. This is in line with the behavior of class I ADH and confirms the stereospecific hydride transfer catalyzed by np-ADH, but is in contrast to UDP-galactose epimerase.

UV−Vis Absorbance of Enzyme-Bound NADH. A small blue shift of 2−5 nm can be attributed to the unstacking of NADH upon binding to A-specific dehydrogenases (the folded NADH from solution binds in an open conformation to the enzyme); however, a larger blue shift is due to specific interactions of NADH with the protein matrix (*7*). The blue shift of 14 nm of np-ADH is comparable to the blue shift of 15 nm of the LADH−NADH binary complex, which is one of the most blue-shifted enzyme−NADH complexes. The near-UV absorbance and CD maxima of NADH bound to UDP-galactose epimerase are red shifted to 345 nm (*5*). The near UV absorbance and circular dichroism maxima are blue shifted to 325 nm for NADH bound to np-ADH.

The 340 nm electronic transition of NADH is proposed to be $\pi-\pi^*$ in nature. In the excited state, charge density increases in the carboxamide group of the dihydronicotinamide. The excited state of dihydronicotinamides is much more polar compared to the ground state, the dipole increases with 6−7 D (*12*, *41*). This is supported by the observation that the NADH absorbance and fluorescence maxima shift to lower wavelength (blue) in apolar solvents (*42*). An empirical linear relationship has been established between the solvent polarity parameter E_T (kcal/mol) and absorbance maxima of dihydronicotinamides bound to dehydrogenases in several binary and ternary complexes, and an estimation of the polarity of the dihydronicotinamide binding site in the enzymes has been made (*11*). Applying this method (*11*) to np-ADH the polarity of the dihydronicotinamide binding site would be comparable to dioxane and toluene ($E_T^{\text{np-ADH}}$ = 34.7 kcal/mol), indicating a very apolar binding environment and being much more apolar compared to other dehydrogenases (lactate dehydrogenase; 47.7 kcal/mol and malate dehydrogenase; 58.0 kcal/mol) (*11*).

Hydrogen bonds of the NADH-carboxamide C═O moiety with solvents and protein surfaces enhance the fluorescence quantum yield and the absorbance extinction coefficient of NADH. Solvents, however, which can act as hydrogen bond acceptor (lone pair donor) to the NADH carboxamide NH_2, cause a small decrease in intensity and a blue shift of absorbance maxima (*42*). The latter is observed (both the blue shift and the lower extinction coefficient) for np-ADH, indicating the possible presence of hydrogen bonding acceptors between the carboxamide NH_2 group and amino acid residues of the enzyme. In LADH, the main-chain carbonyls of residues 317 and 292 have this role. Combining the active site apolarity and the presence of an H-bond acceptor a 14 nm blue shift of NADH absorbance of np-ADH can be accounted for.

Fluorescence of Enzyme-Bound NADH. The 8 nm blue-shift of the NADH fluorescence emission (422 nm), when bound to np-ADH, compared to the LADH−NADH binary complex (430 nm), indicates a larger energy difference between ground state and excited state for np-ADH (since both enzymes have the same excitation maximum). This suggests that the dipole−dipole relaxation affords little stabilization of the polar excited-state NADH by the apolar protein matrix of np-ADH. The NADH binding site of np-ADH is probably more compact and rigid than that of LADH. The fluorescence enhancement of NADH upon binding of

IBA to np-ADH indicates that the inhibitor binds in the np-ADH active site in an orientation similar to that of LADH. A deviation from the LADH topology can, however, be inferred from the negligible energy transfer from tryptophan to NADH in np-ADH whereas significant energy transfer is observed for LADH (*28*). The tryptophan residues in np-ADH are too far away or not in the proper orientation to facilitate efficient energy transfer to NADH. Reduced UDP-galactose epimerase has an emission maximum at 435 nm and an excitation maximum at approximately 340−345 nm, indicating a more polar active site than np-ADH (*4*).

Time-Resolved Fluorescence. Two properties of the NADH fluorescence decay of np-ADH can be distinguished, the very fast fluorescence decay and the broad distribution of fluorescence lifetimes; both properties will be discussed. An excited-state reaction may explain the fast fluorescence decay of NADH bound to np-ADH. This may be electron transfer from the excited-state NADH to an amino acid acceptor, thereby reducing the fluorescence lifetime. In the ground state, the reverse situation takes place restoring the original situation. The average fluorescence lifetime of NADH bound to np-ADH (0.3−0.5 ns) is comparable to that of NADH in solution (0.4 ns, (*13*) and is much shorter than that of other enzyme-bound reduced pyridine dinucleotides including LADH. There are two other dynamic mechanisms possible which explain the decreased fluorescence lifetime of NADH bound to np-ADH: internal conversion and collisional quenching.

(1) Internal Conversion. Because of the small energy difference between the $\pi\pi^*$ and the $n\pi^*$ singlet excited states of nitrogen heterocycles, these states can vibrationally couple, thereby increasing the nonradiative decay rate from the lowest excited state (*43*). The hydrogen-bonding interactions of the NADH carboxamide group are involved in this vibronic coupling (*41*).

(2) Dynamic Quenching. In LADH, the bound dihydronicotinamide moiety is buried deeply in the protein matrix approximately 15 Å from the bulk solvent (*40*). This indicates that nonspecific dynamic quenching from solution is not very probable. Specific residues in the protein, however, are candidates as collisional quenchers. Especially polar residues, such as carboxylic acids, amino groups, and sulfur-containing side chains, can act as dynamic quenchers if they are in close proximity of the dihydronicotinamide ring. At elevated temperatures, side chains and the dihydronicotinamide group have increased thermal motion, the collision probability therefore increases, and this gives rise to a decrease of the fluorescence lifetime. This trend of decrease in fluorescence lifetimes at higher temperatures, which is observed for np-ADH, does not discriminate between the two possible dynamic mechanisms. Both dynamic mechanisms can play a role in governing the excited-state lifetime of both the LADH−NADH binary complex and np-ADH. However, the presence of a polar quenching group in proximity of the nicotinamide ring would cause a much smaller blue shift in the steady-state optical spectra, this is not in line with the observations. But since the arguments are quite qualitative, cancelation of opposing effects cannot be ruled out and a polar residue as quencher might be present.

Recently, it has been suggested that the multiexponential decay of NADH bound to LADH can be interpreted as a reversible excited-state reaction yielding a fluorescent product (*13*). The deviation from monoexponentiality is increased with a decrease in solvent polarity. This observation would be in line with the highly multiexponential fluorescence decay observed for np-ADH. The same authors conclude that in the LADH−NADH binary complex a distribution of lifetimes exists due to the excited-state reaction, in the ternary complex reducing to a finite or even single lifetime. This phenomenon is observed for np-ADH to be even more pronounced than for LADH−NADH. We interpret the excited-state reaction here as electron transfer from excited-state NADH to an amino acid acceptor. The stabilization of the excited state by ternary complex formation of IBA with np-ADH is not due to increased polarity near the nicotinamide ring because no spectral shifts are observed; it appears that the ring is more shielded from the protein matrix by IBA thereby enhancing both steady-state fluorescence intensity and the fluorescence lifetime. Reduced UDP-galactose epimerase has an average fluorescence lifetime of 3.5 ns for the E-NADH−UMP ternary complex and 4.1 ns for the E-NADH−UDP-hexose complex at 25 °C (*4*), indicating much stabilization of the excited-state NADH compared to the ADH−NADH complexes. The fluorescence anisotropy decay experiments on LADH and np-ADH show no mobility of NADH in the active site for both enzymes; the same has been observed for the UDP-galactose epimerase complexes (*4*). For other dehydrogenases, limited flexibility has been observed for enzyme bound NAD(P)H (*8, 11*).

General Conclusions. In conclusion, the study presented here on the nicotinoprotein ADH of *A. methanolica* shows that the active site environment of np-ADH is similar to that of LADH, with respect to nicotinamide binding and inhibitor binding, but that subtle differences can be distinguished. The subtle differences in the substrate binding pocket of both enzymes are reflected in small differences in the inhibition and dissociation constants of the ADH inhibitors, whereas much larger differences are observed with respect to YADH. It appears that the NADH binding environment of the class I ADHs, exemplified by LADH, is unique compared to that of other NAD^+-dependent enzymes and that this is reflected in the blue-shifted optical properties of the ADH bound NADH. Quite the opposite is observed for nicotinoprotein UDP-galactose epimerase which has red-shifted optical properties and a longer NADH fluorescence lifetime. It appears that the nondissociable nature of the NADH in nicotinoproteins is not directly related to the properties of the nicotinamide microenvironment, but is most likely due to multiple interactions involving also the adenine ring, the ribose rings, and the pyrophosphate bridge. The nicotinamide group in both nicotinoproteins is essentially rigidly bound in the active site but displays totally different optical behavior in both enzymes.

ACKNOWLEDGMENT

The authors thank Arie van Hoek for skillful technical assistance with the time-resolved fluorescence measurements.

REFERENCES

1. van Ophem, P. W., and Duine, J. A. (1993) in *Enzymology and molecular biology of carbonyl metabolism 4* (Weiner, H., Crabb, D. W., and Flynn, T. G., Eds.), Plenum press, New York.

2. van Ophem, P. W., van Beuumen, J., and Duine, J. A. (1993) *Eur. J. Biochem. 156*, 819.
3. Wilson, D. B., and Hogness, D. S. (1964) *J. Biol. Chem. 239*, 2469.
4. Wong, S. S., and Frey, P. A. (1977) *Biochemistry 16*, 298.
5. Wong, S. S., Cassim, J. Y., and Frey, P. A. (1978) *Biochemistry 17*, 516.
6. Thoden, J. B., Frey, P. A., and Holden, H. M. (1996) *Biochemistry 35*, 5137.
7. Rizzo, V., Pande, A., and Luisi, P. L. (1987) in *Pyridine Nucleotide Coenzymes* (Dolphin, D., Poulson, R., Avramovic, O., Eds.) p 99, John Wiley, New York.
8. Farnum, M. F., Magde, D., Howell, E. E., Hirai, J. T., Warren, M. S., Grimsly, J. K., and Kraut, J. (1991) *Biochemistry 30*, 11567.
9. Demchenko, A. P. (1994) *Biochim. Biophys. Acta 1209*, 149.
10. Brochon, J. C., Wahl, P., Jallon, J.-M., and Iwatsubo, M. (1976) *Biochemistry 15*, 3259.
11. Baumgarten, B., and Nönes, J. (1988) *Photochem. Photobiol. 47*, 201.
12. Visser, A. J. W. G. (1987) in *Pyridine Nucleotide Coenzymes* (Dolphin, D., Poulson, R., Avramovic, O., Ed.) pp 163, John Wiley, New York.
13. Ladokhin, A. S., and Brand, L. (1995) *J. Fluoresc. 5*, 99.
14. Gafni, A., and Brand, L. (1976) *Biochemistry 15*, 3165.
15. Kierdaszuk, B., Malak, H., Gryczynski, I., Callis, P., and Lakowicz, J. R. (1996) *Biophys. Chem. 62*, 1.
16. Visser, A. J. W. G., and Van Hoek, A. (1981) *Photochem. Photobiol. 33*, 35.
17. Krishnamoorthy, G., Periasamy, N., and Venkataraman, B. (1987) *Biochem. Biophys. Res. Commun. 144*, 387.
18. Laemmli, U. K. (1970) *Nature 227*, 680.
19. Dunn, M. F., and Bernard, S. A. (1971) *Biochemistry 10*, 4569.
20. Cornish-Bowden, A. (1995) *Analysis of enzyme kinetic data*, Oxford University Press, Oxford.
21. van Iersel, J., Frank Jzn, J., and Duine, J. A. (1985) *Anal. Biochem. 151*, 196.
22. Provencher, S. W., and Glöckner, J. (1981) *Biochemistry 20*, 33.
23. Bastiaens, P. I. H., van Hoek, A., Benen, J. A. E., Brochon, J. C., and Visser, A. J. W. G. (1992) *Biophys. J. 63*, 839.
24. Pap, E. H. W., Bastiaens, P. I. H., Borst, J. W., van den Berg, P. A. W., van Hoek, A., Snoek, G. T., Wirtz, K. W. A., and Visser, A. J. W. G. (1993) *Biochemistry 32*, 13310.
25. Livesey, A. K., and Brochon, J. C. (1987) *Biophys. J. 52*, 693.
26. Yonetani, T., and Theorell, H. (1962) *Arch. Biochem. Biophys. 99*, 433.
27. Plapp, B. V., Eklund, H., and Branden, C. (1978) *J. Mol. Biol. 122*, 23.
28. Abdallah, M. A., Biellmann, J.-F., Wiget, P., Joppich-Kuhn, R., and Luigi, P. L. (1978) *Eur. J. Biochem. 89*, 397.
29. Vos, K., van Hoek, A., and Visser, A. J. W. G. (1987) *Eur. J. Biochem. 165*, 55.
30. Couprie, M. E., Mérola, F., Tauc, P., Garzella, D., Delboulbé, A., Hara, T., and Billardon, M. (1994) *Rev. Sci. Instrum. 65*, 1485.
31. Davis, G. J., Bosron, W. F., Stone, C., Owusu-Dekyi, K., and Hurley, T. D. (1996) *J. Biol. Chem. 271*, 17057.
32. Gould, R. M., and Plapp, B. V. (1990) *Biochemistry 29*, 5463.
33. Stone, C. L., Bosron, W. F., and Dunn, M. F. (1993) *J. Biol. Chem. 268*, 892.
34. Shearer, G. L., Kim, K., Lee, K. M., Wang, C. K., and Plapp, B. V. (1993) *Biochemistry 32*, 11186.
35. Thoden, J. B., Frey, P. A., and Holden, H. M. (1996) *Biochemistry 35*, 2557.
36. Park, D. H., and Plapp, B. V. (1991) *J. Biol. Chem. 266*, 13296.
37. Kovár, J., Simec, K., Kucera, I., and Matyska, L. (1984) *Eur. J. Biochem. 139*, 585.
38. Bränden, C.-I., Jörnvall, H., Eklund, H., and Furugren, B. (1975) in *The Enzymes* (Boyer, P. D., Ed.) pp 103, Academic Press, New York.
39. Rétey, J., and Robinson, J. A. (1982) *Stereospecificity in organic chemistry and enzymology*, Vol. 13, Verlag Chemie, Weinheim.
40. Eklund, H., Samama, J.-P., and Jones, T. A. (1984) *Biochemistry 23*, 5982.
41. Deng, H., Zheng, J., Sloan, D., Burgner, J., and Callender, R. (1989) *Biochemistry 28*, 1525.
42. Fischer, P., Fleckenstein, J., and Hönes, J. (1988) *Photochem. Photobiol. 47*, 193.
43. Lim, E. C. (1986) *J. Phys Chem. 90*, 6770.

BI972115U